ARTICLE **OPEN**

Check for updates

Aerosol high water contents favor sulfate and secondary organic aerosol formation from fossil fuel combustion emissions

Xiaojuan Huang[1,8], Zhe Liu [1,8], Yanzhen Ge[2✉], Qing Li [1], Xiaofei Wang [1], Hongbo Fu[1], Jian Zhu[1], Bin Zhou[1], Lin Wang [1], Christian George [1,3], Yan Wang[4], Xinfeng Wang [4], Jixin Su[4], Likun Xue[4], Shaocai Yu[5], Abdewahid Mellouki[6] and Jianmin Chen [1,7✉]

Fine-particle pollution associated with high sulfate and secondary organic aerosol (SOA) contents still occurs in winter, despite considerable reductions in precursor emissions in China. The chemical mechanisms involved are consistently acknowledged to be linked with aerosol water but remain poorly understood. Here, we present findings demonstrating that the synergistic effect of elevated aerosol water content and particles originating from fossil fuel combustion significantly enhanced the rapid formation of sulfate and SOAs under high humidity conditions during winter in northern China. The presence of high aerosol water content promoted the aging process of particles containing elemental carbon (EC) and facilitated the formation of SOAs. Evidence from single particles reveals an increased potential for SOA formation from primary organic aerosols (POAs) originating from fossil fuel combustion, in the presence of increasing aerosol water. Under conditions of relative humidity exceeding 85%, the multiphase oxidation of SO_2 by in-particle nitrite/nitrous acid, generated through reactions involving aged EC-containing and iron-rich particles, as well as aqueous-phase formation of hydroxymethanesulfonate (HMS), led to a substantial increase in sulfate production. This study emphasizes the critical role of aerosol water in the aerosol chemistry concerning sulfate and SOAs, highlighting the urgent necessity to mitigate primary emissions from fossil fuel combustion.

INTRODUCTION

Severe haze pollution has been effectively alleviated in China due to the substantial reduction in primary air pollutant emissions over the past two decades[1]. Nevertheless, during winter, rapid formation of sulfate and secondary organic aerosol (SOA) still occurs, exacerbating the development of severe haze[2–4]. The formation of sulfate is governed by intricate and robust chemical feedback associated with oxidants, aerosol pH, and meteorological conditions[5]. Sulfate can be formed through various pathways of SO_2 oxidation, including gas-phase oxidation by hydroxyl radical (OH), aqueous-phase oxidation involving H_2O_2, O_2 catalyzed by transition-metal ions (TMI), NO_2, and organic hydroperoxides[6–9]. The air quality models incorporating these oxidation pathways still fail to adequately address the observed rapid SO_2 oxidation chemistry, and the missing sulfate is likely attributed to multiphase oxidation processes involving aerosol water[3,7]. SOAs are formed either through the condensation of gas-phase oxidized organic compounds with low volatility onto particles[4,10] or via particle-phase oxidation processing[11,12]. These two pathways were influenced by various factors associated with uptake and chemical reactions, including ambient relative humidity (RH), aerosol liquid water content (LWC), aerosol pH, and ambient temperature[13]. The enhanced formation of SOAs, an overwhelming composition of organic aerosols (OAs) during haze pollution, is primarily attributed to favorable chemical processes facilitated by increasing aerosol water[2,4,14,15].

Aerosol water, acting as both a medium and reactant in the multiphase reactions, exerts significant influence on gas-particle transformations through intricate physical and chemical mechanisms[16–18]. An increase in aerosol water thermodynamic reversibly favors the dissolution of reactive inorganic or organic gases into the aqueous phase by elevating their effective Henry's law constants, and irreversibly drives gas uptake by enhancing in-particle reactions[19,20]. The dominant mechanisms responsible for sulfate formation exhibit dynamic evolution, influenced by factors such as LWC, aerosol pH and oxidants[7]. In conditions characterized by high LWC and weakly acidic or neutral aerosol pH (>5.5), the aqueous oxidation of SO_2 by dissolved NO_2 and nitrous acid (HONO) is favored[21]; whereas manganese-catalyzed oxidation on particle surfaces predominates in sulfate formation under low LWC and a pH range of 4–5[8,22]. Aerosol water also facilitates surface-mediated processes, potentially by creating aqueous solution environments on the surface and thereby lowering the energy barrier of reactions, or by providing a bridge for electron-transfer reactions[23]. In wet particles, hydrophobic elemental carbon (EC) can actively participate in in-particle chemical processes and effectively catalyze the oxidation of SO_2[24]. For SOAs, the presence of aerosol water may play a crucial role in modulating precursors partitioning into the liquid phase and facilitating their oxidation

[1]Shanghai Key Laboratory of Atmospheric Particle Pollution and Prevention (LAP3), Department of Environmental Science & Engineering, Institute of Atmospheric Sciences, Fudan University, Shanghai 200438, China. [2]Tai'an Ecological Environment Protection and Control Center, Tai'an Ecological Environment Bureau, Tai'an 271000, China. [3]University of Lyon, Université Claude Bernard Lyon 1, CNRS, IRCELYON, F-69626 Villeurbanne, France. [4]School of Environmental Science and Engineering, Research Institute of Environment, Shandong University, Qingdao 266237, China. [5]Key Laboratory of Environmental Remediation and Ecological Health, Ministry of Education, College of Environmental and Resource Sciences, Zhejiang University, Hangzhou 310058, China. [6]Institut de Combustion, Aérothermique, Réactivité et Environnement, CNRS, 45071, Orléans CEDEX 02, France. [7]Institute of Eco-Chongming (IEC), 3663 N. Zhongshan Rd., Shanghai 200062, China. [8]These authors contributed equally: Xiaojuan Huang, Zhe Liu. ✉email: tahbj@163.com; jmchen@fudan.edu.cn

within the aqueous phase, thereby dynamically influencing SOA formation[4,10,14]. Improving the understanding of aerosol water and its potential role in sulfate and SOA formation is crucial for elucidating the fundamental chemical processes governing haze pollution, particularly during winter when atmospheric oxidation capacity is relatively limited.

In this study, we conducted comprehensive field observations to characterize the aerosol chemical components in terms of both bulk and single particles during winter. The field study was conducted through the synchronous use of online instruments, including ion chromatography (IC) systems, single particle aerosol mass spectrometer (SPAMS), and differential optical absorption spectroscopy (DOAS), during Jan.–Feb. 2022 in Tai'an, a city at the foot of Mount Tai that is affected by the vagaries of weather in northern China[25,26]. Our findings revealed that elevated LWC and fossil fuel combustion emissions synergistically contributed to the enhanced sulfate and SOA formation under high RH conditions during winter. This study advances our understanding of the primary drivers behind the formation of secondary aerosols during winter haze pollution and provides valuable insights for devising effective mitigation strategies.

RESULTS

Particle pollution processes evolve with humidity and emissions

Five particle growth episodes (labeled as Ep *I* to *V* and depicted with circles in Fig. 1a) occurred during the observation period, all exhibiting dynamic evolutions in response to variations in RH (Supplementary Fig. 1). Compared with the low average RH of 32% during the clean period (Cp), the RH values during Ep *I* to *V* were 88%, 64%, 56%, 45%, and 42%, respectively (Fig. 1b). Highly consistent with these RH levels, the average PM$_{2.5}$ mass concentrations during Ep *I* to *V* were 104.7, 101.7, 81.7, 50.9, and 48.9 μg m^{-3}, respectively, representing 2.0–4.3 times that during Cp. However, an inconsistency was observed between the mass concentration and particle number (*N*) of PM$_{2.5}$ in the five pollution episodes. This discrepancy may be attributed to differentiated physical and chemical processes governing particle formation between these episodes, which were driven by differences in RH and manifested by distinctive single particle types and particle sizes (Fig. 1c and Supplementary Figs. 1–3).

The single particles collected using SPAMS in this study revealed the ubiquitous presence of particles containing EC, which constitutes a complex mixture of compounds formed from incomplete combustion of diverse fuels (e.g., predominantly coal, gasoline and diesel vehicles, and biomass in China)[27–29]. The EC-containing particles constituted an average proportion of 62% of the total particles and reached up to 75% during Ep *I*, highlighting the significant contribution of fuel combustion activities to winter haze pollution in Tai'an city. Under varying atmospheric conditions, these EC-containing particles would undergo diverse degrees of aging, thereby exerting intricate influences on the atmospheric physical and chemical processes, environment, and climate. The number fraction of fresh and aged EC-containing particles (defined in "Methods" section and characterized in Fig. 1c) responded oppositely to variations in RH. The aged EC-containing particles accounted for 59% and 45% of total particles during Ep *I* and *II*, respectively, whereas they constituted a minority during Cp (16%). These aged particles were likely primarily derived from the aging process of fresh EC-containing particles, either through hygroscopic growth and heterogeneous reactions on particle surfaces or via aqueous-phase processing in particle droplets. Moreover, on average, the fossil fuel combustion-derived POAs (namely ECOCCN particles, abbreviated as FC-POAs in "Methods" section) accounted for 70% of the total combustion-derived POAs (i.e., the sum of ECOCCN and KOCCN),

while biomass burning derived POAs (namely KOCCN particles, defined in "Methods" section) constituted 30%. During Ep *I* and Ep *II*, FC-POAs exhibited a fractional contribution of 83% and 75%, respectively, which was significantly higher than other periods (ranging from 64% to 69%). These results imply a crucial role of fuel combustion, particularly that of fossil fuels, in the formation of winter haze pollution.

Comparable PM$_{2.5}$ mass concentrations were observed during Ep *I* and *II*, yet their chemical compositions exhibited distinct characteristics. This distinction was primarily manifested by the explosive growth of SO$_4^{2-}$ but constant NO$_3^-$ mass concentration during Ep *I*, whereas Ep *II* witnessed a cumulative formation of NO$_3^-$ dominating the composition with a slow increase in SO$_4^{2-}$ (Supplementary Fig. 1). There are two primary factors contributing to this distinction. Firstly, the RH was higher during Ep *I* compared to Ep *II*. The sustained elevated RH (>85%) during Ep *I* largely promoted moisture uptake of particles. Under such high RH conditions, heterogeneous and aqueous chemical processes were strengthened, as evidenced by the presence of larger particle sizes and a significant amount of particles containing hydroxymethanesulfonate (HMS; *m/z* −111[HOCH$_2$SO$_3^-$]) during Ep *I* (Supplementary Figs. 1 and 4). Secondly, during Ep *I*, there was a higher abundance of EC-containing and Fe-rich particles (particularly those containing oxalate) compared to Ep *II* (Supplementary Figs. 1 and 4). These particles may have facilitated the oxidation of SO$_2$[24,30], leading to the rapid formation of secondary sulfate. In addition, periods with low RHs also exhibited a high particle number despite a low mass concentration of sulfate. During these periods, a large proportion of the sulfate may have originated from fresh emissions from combustion, as indicated by the higher fractions of ECOCCN and KOCCN particles, which exhibited prominent peaks at *m/z* −97[HSO$_4^-$] in their mass spectra (Fig. 1d).

Enhancement of aerosol water and sulfate driven by high humidity

The aerosol LWC exhibited an exponential increase with rising RH, and this increase was more sharply at higher levels of secondary inorganic aerosols (SIAs; i.e., sulfate, nitrate, and ammonium) (Fig. 2a). Notably, the LWC doubled as the RH increased from 80–85% to 85–90% (Fig. 2b). This indicates the existence of a positive feedback loop triggered by elevated RH between particle hygroscopicity, LWC, and hydrophilic chemical components (i.e., inorganic and water-soluble organic aerosols), which eventually yields high concentrations of PM$_{2.5}$[31]. The viscosity and diffusivity of reactive substances highly depend on RH[32]. As RH increases and approaches or exceeds the deliquescence RH (DRH) of inorganic species, a moisture-induced phase transition from a semisolid state to a liquid state occurs in the particles[31,33]. The DRH values of NH$_4$NO$_3$ and (NH$_4$)$_2$SO$_4$ are 76.6% and 81.8%[33], respectively, at 0 °C, which is close to the mean temperature during the field study period. It is worth noting that the phase state transition occurs at RH values slightly below the DRH due to the presence of multicomponent mixtures in atmospheric particles[33,34]. An RH of approximately 68% was reported as a threshold of transition from a semisolid to liquid state in winter in Beijing[35]. The presence of liquid-state particles can facilitate the uptake, mass transfer and multiphase chemical reactions of reactive trace gases, thereby promoting the formation of secondary aerosols and facilitating rapid growth in both aerosol mass and LWC; in turn, this facilitation can be further enhanced as the LWC increases[31,36]. Both Ep *I* and *II* developed under high RH conditions and were accompanied by obvious increases in the LWC and SIAs (Supplementary Fig. 5). During Ep *I*, the RH remained approaching 90%, indicating a liquid state of the particles and their ability to absorb abundant water. In contrast, during Ep *II*, the RH exhibited a gradual increase from 39% to 86%,
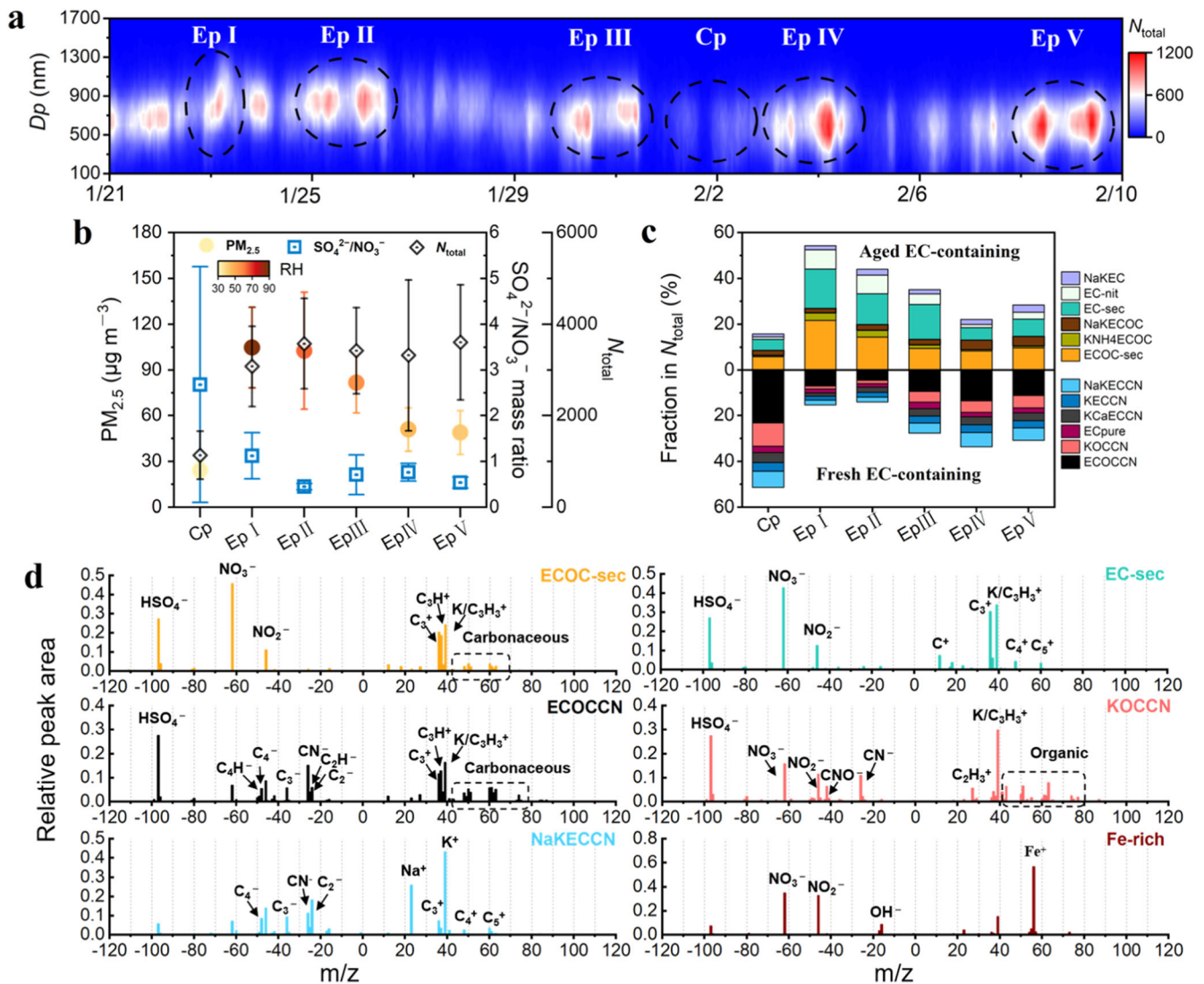
Fig. 1 Chemical characteristics of particles during the winter observation period from Jan. 21 to Feb. 10, 2022. a Temporal profile of size-resolved total particle number (N_{total}) distributions. Dp denotes the particle diameter, while Cp and Ep I–V denote the clean period and particle growth episodes, respectively. **b** The differences in $PM_{2.5}$ mass, N_{total}, SO_4^{2-}/NO_3^- mass ratio, and RH between the Cp and Ep I–V. The marker and variation bar represent the mean and standard deviation of each group. **c** Number fraction of aged and fresh EC-containing particle types during Cp and Ep I–V. **d** Mass spectra of specific particle types.

indicating a potential phase transition from a semisolid to a liquid state due to the reduction in particle rebound fraction under increasing LWC and SIAs[31,36]. This may account for the lower LWC observed during Ep II compared to Ep I, despite comparable SIAs concentrations between the two periods (Supplementary Figs. 1 and 5).

The explosive growth of sulfate necessitates high RH conditions[37,38], under which the generation of sulfate and LWC can establish an efficient positive feedback loop. Figure 2b shows that a sharp increase in the SO_4^{2-} mass occurred in the RH bin of 85–90% (increased by 60% compared to that at 80–85%), below which SO_4^{2-} responded sluggish to RH variations. However, the feedback loop for nitrate could potentially be initiated at a lower RH, as indicated by the higher sensitivity of NO_3^- mass to RH compared to that of sulfate when RH was below 70% (Fig. 2b). This discrepancy can be attributed to the distinct formation mechanisms of SO_4^{2-} and NO_3^-. The LWC and SO_4^{2-} were strongly correlated ($r = 0.901$, $p < 0.01$ by two-tailed t-test), and both drastically increased at RH of 85–90%. The molar ratio of $[SO_4^{2-}]/$ $[SO_2]$ positively responded to the enhanced LWC (Supplementary

Fig. 6), emphasizing the crucial role played by aerosol water in facilitating the oxidation of SO_2. Nevertheless, the response of nitrate to LWC exhibited distinct characteristics; specifically, when the LWC exceeded approximately 100 µg m^{-3} (Ep I), there was only a marginal change in the $[NO_3^-]/[NO_2]$ ratio with further increases in LWC (Supplementary Fig. 6). In the ammonia-rich atmosphere of Tai'an (indicated by G-ratio >1.0[39], calculated in Supplementary Note), the nitrate oxidation pathways were probably inhibited by insufficient photochemical oxidants during Ep I, resulting in a limited response of NO_3^- to variations in LWC.

High aerosol water promotes HMS and FC-POA-derived SOA formation

High LWC facilitated the aging of EC-containing particles. The number of aged EC-containing particles ($N_{aged\ EC-containing}$) exhibited a continuous and pronounced increase in response to increasing RH (Fig. 2b). $N_{aged\ EC-containing}$ increased more steeply than $N_{fresh\ EC-containing}$, which declined when the RH exceeded ~65%, suggesting that the aging of EC-containing particles was further strengthened at high RH. The observed mass
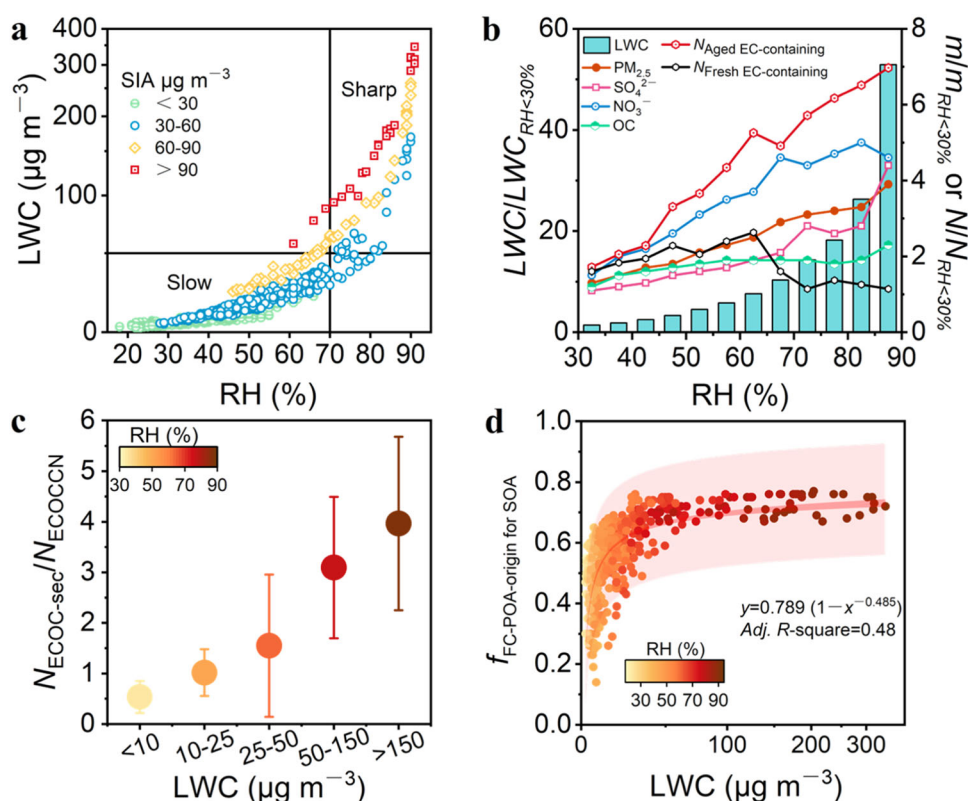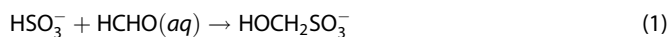
Fig. 2 Chemical evolution of aerosol particles under the influence of humidity. a The LWC as a function of RH. The LWC are grouped according to SIA concentrations in the $PM_{2.5}$. **b** The ratio of the chemical species in the RH bins with a 5% interval to those at the condition of RH < 30%. **c** The ratio of the ECOC-sec to ECOCCN particle numbers for the different LWC bins. The circles are colored according to the RH, while the variation bar represents the standard deviation within each group. **d** Number fraction of SOAs derived from FC-POAs as a function of LWC.

concentration of OC in units of $\mu gC\ m^{-3}$ weakly responded to the increasing RH or LWC. However, the OAs, which may contain elements such as oxygen (O), nitrogen (N), sulfur (S), and phosphorus (P) in addition to carbon (C) and hydrogen (H), likely underwent significant changes in terms of their mass concentration and chemical composition. This can be inferred from the observed increases in both the number and particle size of ECOC-sec particles (Supplementary Figs. 1 and 3). During Ep I, a rapid formation of HMS, a tracer for aqueous-phase chemistry and aqueous SOA formation, was observed, which is known to result from reactions between bisulfate (HSO_3^-) and sulfite (SO_3^{2-}) with dissolved formaldehyde (HCHO) in the aqueous phase (Eqs. 1 and 2)[40–44]. In the aerosol pH range of 3.3–4.3 during Ep I (Supplementary Fig. 5), nearly all dissolved SO_2 (referred to as S(IV)) predominantly existed as HSO_3^-[33], indicating that the reaction between HSO_3^- with HCHO might play a dominant role in HMS formation. However, the HCHO-SO_3^{2-} reaction pathway cannot be disregarded given its significantly higher reaction rate constant (approximately five orders of magnitude) compared to that of HCHO-HSO_3^-[33,43].

$$HSO_3^- + HCHO(aq) \rightarrow HOCH_2SO_3^- \qquad (1)$$

$$SO_3^{2-} + HCHO(aq) + H_2O \leftrightarrow HOCH_2SO_3^- + OH^- \qquad (2)$$

HMS was the principal organosulfur species detected via the SPAMS in this study and probably a significant contributor to the SOA mass during Ep I. Approximately 50% of the HMS-containing particles were distributed in the ECOC-sec and EC-sec particles, with two distinct subtypes rich in HMS identified as ECOC-HMS and EC-HMS (Supplementary Figs. 1 and 2). The highest numbers and fractions of the ECOC-HMS and EC-HMS particles were

observed at 07:00 on Jan. 23 (LWC: 201 $\mu g\ m^{-3}$, RH: 89%), accounting for 17% and 21% of the ECOC-sec and EC-sec particles, respectively. This suggests that the ECOC-sec and EC-sec particles may have undergone aqueous-phase processes, along with the formation of HMS.

The ECOCCN and ECOC-sec were the predominant particles in ECOC-fresh and ECOC-aged particles (defined in "Methods" section), accounting for 70% and 67%, respectively. The relative abundance of these two particle types exhibited opposite temporal variations (Supplementary Fig. 1) and reacted oppositely to variations in LWC. The $N_{ECOC-sec}/N_{ECOCCN}$ ratio increased significantly with increasing LWC, ranging from 0.5 (LWC < 10) to 1.6 (LWC 25–50) and reaching up to 4.0 (LWC > 150 $\mu g\ m^{-3}$) (Fig. 2c). This observation implies that ECOCCN particles acted as precursors for ECOC-sec particles, serving as either the medium or reactants for their formation. As described in "Methods" section, ECOCCN particles were identified as FC-POAs, while ECOC-sec particles were identified as SOAs. The classification of ECOC-sec particles as SOAs was primarily based on the following reasons. Firstly, 57% of ECOC-sec particles contained ions indicative of oxidized organic species, i.e., +43[$C_2H_3O^+$], −45 ([CHO_2^-] or [$CH_3CH_2O^-$]), −59 ([$CH_3CO_2^-$] or [$CH_3CH_2CH_2O^-$]), −73 ([$CH_3CH_2CO_2^-$] or [$CHOCO_2^-$]), −87[$CH_3COCO_2^-$], and −89[$HC_2O_4^-$][42]. Secondly, aqueous HMS formation preferentially occurred in the ECOC-sec particles, i.e., 48% of ECOC-sec particles were mixed with HMS during the period of high HMS production from 00:00 to 12:00 on Jan. 23. Thirdly, ECOC-sec particle number was positively correlated with LWC ($r = 0.607$, $p < 0.01$ by two-tailed t-test). These results implied that the formation of ECOC-sec particles involved aqueous processes.

The FC-POAs origin of SOAs was dominant at high LWC, as manifested by the fact that the $f_{FC-POA\ origin\ for\ SOA}$ (calculated in "Methods" section) showed a power exponential growth with
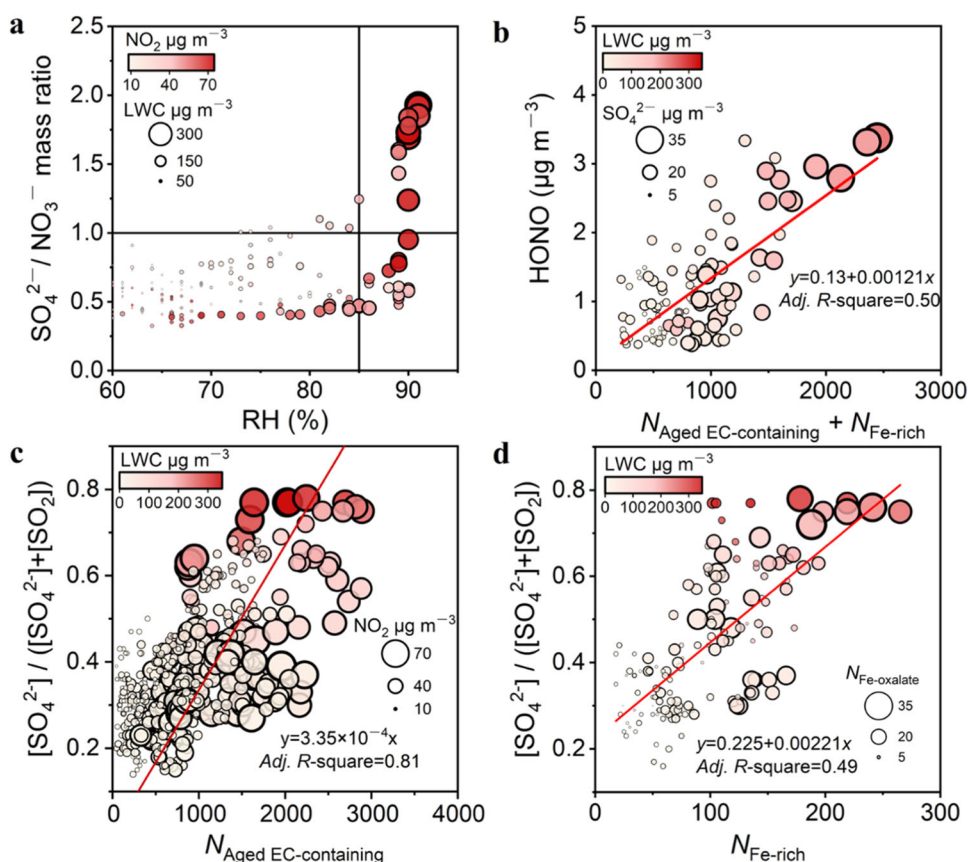
Fig. 3 Analysis of the factors determining sulfate formation. a Mass ratio of SO_4^{2-}/NO_3^- as a function of RH. The circles are colored according to NO_2 concentration, and circle sizes are scaled to LWC. **b** Gaseous HONO as a function of the sum of $N_{aged\ EC-containing}$ and $N_{Fe-rich}$ from Jan. 21 to 26 covering Ep *I* and *II*. The circles are colored and sized according to LWC and SO_4^{2-}, respectively. **c** The ratio of $[SO_4^{2-}]/([SO_4^{2-}] + [SO_2])$ as a function of $N_{aged\ EC-containing}$ throughout the campaign. The circles are colored and sized according to LWC and NO_2, respectively. **d** The ratio of $[SO_4^{2-}]/([SO_4^{2-}] + [SO_2])$ as a function of $N_{Fe-rich}$ from Jan. 21 to 26. The circles are colored and sized according to LWC and $N_{Fe-oxalate}$, respectively.

increasing LWC (Fig. 2d). For LWC below ~50 µg m^{-3}, the $f_{FC-POA\ origin\ for\ SOA}$ exhibited an almost linear response to LWC, increasing from 0.46 to 0.56 to 0.66 as the LWC bin increased from <10 to 10–25 to 25–50 µg m^{-3}. However, the $f_{FC-POA\ origin\ for\ SOA}$ exhibited a slow increase and remained nearly constant when the LWC exceeded ~50 µg m^{-3}, with average values of 0.71 and 0.73 for the LWC bins of 50–150 and >150 µg m^{-3}, respectively. The FC-POAs (i.e., ECOCCN) have a certain degree of hygroscopicity due to their organic coating and primary sulfate carrying capacity (Fig. 1d). They provide an efficient medium for the uptake of gas-phase oxygenated compounds or reactive organic/inorganic gases, and the subsequent surface- or aqueous-phase reactions within the aquifer of the POA particles. Moreover, they may act as reactants, undergoing aqueous-phase chemical transformation to form SOAs. A previous study has reported a rapid aqueous-phase transformation of fossil fuel-derived POAs containing polycyclic aromatic hydrocarbons (PAHs) into SOAs, which can explain 20% of the observed OAs during a Beijing haze period[12].

Multiphase oxidation of SO_2 by in-particle N(III) promoted by aerosol water

The rapid production of sulfate during Ep *I* was attributed to the simultaneous generation of both inorganic sulfate and HMS. A high yield of HMS was exclusively observed during Ep *I*, which perfectly satisfied the prerequisites for HMS generation and preservation in the atmosphere, including high LWC, moderately acidic pH, low temperatures, and weak photochemical activity[45]. The stability of HMS is largely pH-dependent; that is, it remains

stable at pH < 6 but dissociates at higher pH values[46,47]. In the presence of strongly alkaline eluent during conventional IC measurements, HMS dissociates rapidly into HCHO and SO_3^{2-}, and the produced SO_3^{2-} can be rapidly oxidized to SO_4^{2-} by dissolved oxidants (e.g., O_2, OH)[46,47]. Consequently, HMS can potentially be misinterpreted as inorganic sulfate[45,46]. The average ratio of HMS/HSO4 in peak area during the high HMS generation period (from 2:00 to 13:00 on Jan. 23) in Ep *I* was found to be 0.08, ranging from 0.04 to 0.12. These ratios were very close to those obtained in a quantitative study conducted during winter pollution in Beijing, which reported that HMS accounted for ~10% of the sulfate with molar ratios of HMS/sulfate ranging from 0.02 to 0.12[48]. This suggests that the HMS made a non-negligible contribution to the observed high SO_4^{2-} mass detected by IC with alkaline eluent during this pollution period, potentially representing a missing source of sulfur in winter haze of northern China.

In addition to a certain contribution arising from the misjudgment of HMS, the rapid production of sulfate during Ep *I* was predominantly ascribed to the formation of inorganic sulfate. The weak photochemical reactivity, as indicated by the low daytime O_3 concentration, inhibited the SO_2 oxidation pathways mediated by the oxidants of photolytic origin, i.e., $S(IV) + OH/O_3/H_2O_2$[49]. Although the SO_4^{2-}/NO_3^- mass ratio actively responded to NO_2 and LWC (Fig. 3a), the aqueous oxidation of dissolved SO_2 by NO_2 was not favored under moderate aerosol acidity conditions (particularly with aerosol pH of 4.0–4.5 at RH > 85%) in this study, since this reaction pathway predominates in weakly acidic or neutral solutions (pH > ~6)[3,50]. Instead, in-particle nitrite/nitrous
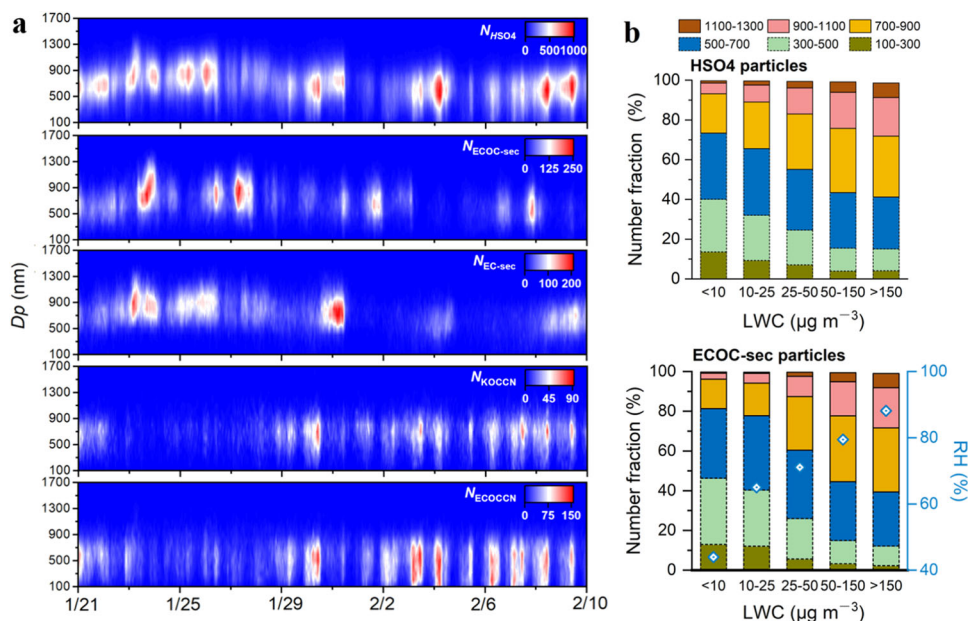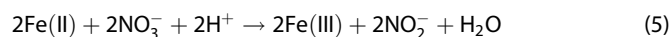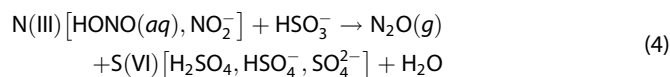
Fig. 4 Response of particles in different sizes to time and LWC. a Time series of the particle size distribution for HSO4, ECOC-sec, EC-sec, KOCCN, and ECOCCN particles. **b** Number fractions of HSO4 and ECOC-sec particles in different size segments (nm) in response to different LWC bins.

acid ((N(III); i.e., NO_2^- and aqueous HONO) that generated from the reactions involving aged EC-containing and Fe-rich particles probably drove the fast kinetics of SO_2 oxidation into SO_4^{2-}. This inference is supported by the concurrent presence of high values of SO_4^{2-}, LWC, HONO, aged EC-containing, and Fe-rich particles (Supplementary Fig. 5), as well as the linear increase in HONO response to an increasing number of aged EC-containing and Fe-rich particles (Fig. 3b).

The oxidation of SO_2 to SO_4^{2-} positively responded to the increase in the aged EC-containing particles and exhibited a high transformation rate under the condition of concurrently high LWC and high NO_2 (Fig. 3c). The EC-catalytic SO_2 oxidation chemistry may involve the initial generation of HONO through the reaction of NO_2 on EC particles (Eq. 3) and subsequent aqueous reactions between in-particle N(III) and HSO_3^- to produce sulfate (Eq. 4).

$$NO_2(g) + \{EC\}_{surface} \rightarrow \{EC\}_{surface} + HONO + other\ product \quad (3)$$

$$\begin{aligned} N(III)\left[HONO(aq), NO_2^-\right] + HSO_3^- &\rightarrow N_2O(g) \\ + S(VI)\left[H_2SO_4, HSO_4^-, SO_4^{2-}\right] + H_2O \end{aligned} \quad (4)$$

$$2Fe(II) + 2NO_3^- + 2H^+ \rightarrow 2Fe(III) + 2NO_2^- + H_2O \quad (5)$$

where the brackets {} denote particle surface sites. Equation 3 comprises two sequential steps, namely, the physical absorption of NO_2 by EC particles and the subsequent generation of HONO through extraction of an allylic hydrogen by NO_2 at the reducing surface sites of the EC particles[24]. The HONO production process is the rate-limiting step of this mechanism[24]. This sulfate formation mechanism has been documented in previous studies and has been reported to depend strongly on NO_2, NH_3, and RH and to depend weakly on the SO_2 concentration[24]. Among the aged EC-containing particles, HONO exhibited a closer relationship with ECOC-aged particles ($r = 0.588$, $p < 0.01$ by two-tailed t-test) than with EC-aged particles ($r = 0.455$, $p < 0.01$ by two-tailed t-test). The coating of organic acids on the EC particles could enhance the NO_2 uptake and thereby increase the HONO yield[24,51].

TMIs, specifically Fe(III) and Mn(II), are effective catalysts for S(IV) in solutions[8,9,13]. Fe ($m/z = 56$) was the primary TMI detected using SPAMS, with a distinct identification of Fe-rich particle type, while

the detected Mn ($m/z = 55$) was very low. The oxidation of SO_2 by O_2, catalyzed by Fe(III), can be inhibited by high ionic strength and sulfate concentraions[7,13]. Given the substantial generation of SIAs during Ep I, it is unlikely that this pathway assumed a dominant role. HONO exhibited positive correlations with the number of Fe-rich ($r = 0.607$, $p < 0.01$ by two-tailed t-test) and Fe-oxalate particles ($r = 0.599$, $p < 0.01$ by two-tailed t-test; see Supplementary Fig. 4 for mass spectrum and particle number), indicating the production of in-particle N(III). Oxalate represents one of the most abundant and potent organic ligands for Fe(III) in the atmosphere, with its formation being enhanced by particles containing Fe and further facilitated by high RH[52]. Particles containing Fe can absorb gaseous HNO_3 or HONO to generate nitrate, and subsequently, under acidic conditions, the Fe dissolves and mixes with the nitrate. This was confirmed by a high intensity of $m/z\ -62[NO_3^-]$ and $-46[NO_2^-]$ observed in the mass spectrum of the Fe-rich particles (Fig. 1d). The photolysis of Fe(III)-oxalate complexes generates Fe(II), which subsequently reduces nitrate to N(III) and regenerates Fe(III) (Eq. 5)[30]. Then the N(III) oxidizes the dissolved SO_2 to generate sulfate (Eq. 4). The oxidation of SO_2 to SO_4^{2-}, as depicted in Fig. 3d, positively responded to the increase in the Fe-rich and Fe-oxalate particles, and this oxidation process was enhanced in the presence of high LWC.

These two catalytic oxidation pathways leading to the explosive growth of sulfate predominantly occurred in larger particle sizes. During Ep I, both ECOC-sec and EC-sec particles demonstrated significant growth within the particle size range of 700–1300 nm, which aligns with that of HSO4 particles (Fig. 4a). The 700–1300 nm HSO4 particles exhibited strong correlations with SO_4^{2-}, LWC, RH, HONO, ECOC-sec, EC-sec, and Fe-rich particles and displayed enhanced correlations with increasing size (Supplementary Fig. 7). In response to the increasing LWC, there was an increase in the fraction of 700–1300 nm HSO4 particles (Fig. 4b), indicating aerosol water-driven sulfate formation. Similar variations in particle size distributions with LWC were also observed for ECOC-sec particles, reflecting their aqueous-phase formation processes. In contrast, 100–700 nm HSO4 particles dominated at low LWC. Similar temporal variations in the particle number of 100–700 nm HSO4, ECOCCN and KOCCN particles further supported their primary origin.
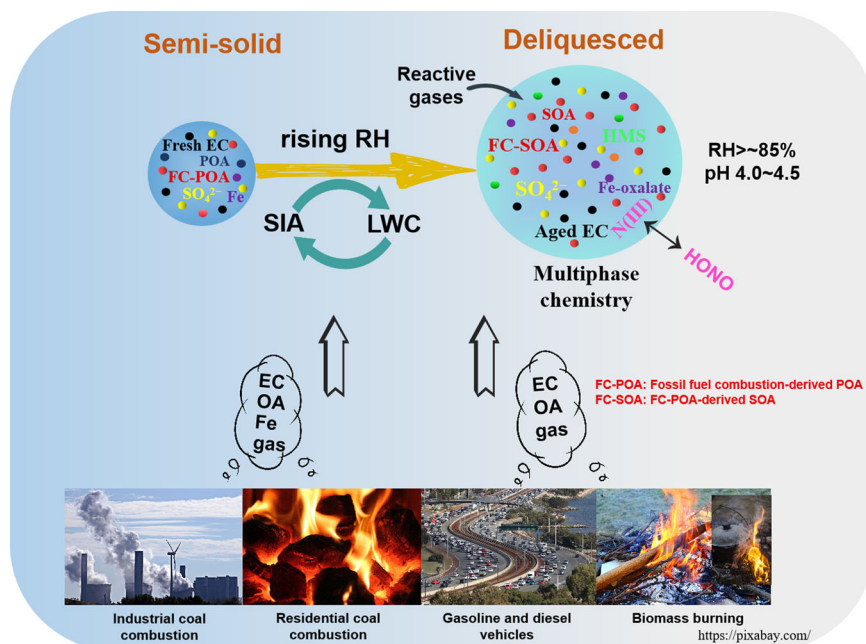
Fig. 5 Conceptual diagram depicting sulfate and SOA formation in deliquesced particles. High aerosol water triggered by extremely high RH drives the secondary transformation of primary emissions emitted from the combustion of fuels, particularly fossil fuels. The images presented in this figure are downloaded from the website of https://pixabay.com/.

DISCUSSION

This study provides explanations for the puzzling occurrences of wintertime haze pollution with high yields of sulfate and SOAs, despite low SO_2 levels and weak photochemical conditions. We revealed two crucial factors, i.e., precursors emitted from fuel combustion and elevated aerosol water triggered by high humidity. Fuel combustion releases complex mixtures of gaseous pollutants (i.e., SO_2, NOx, CO, NH_3 and volatile organic compounds), primary carbonaceous particles (i.e., EC and POAs), metal minerals, and ash into the atmosphere. In winter of northern China, substantial solid fuels (e.g., coal, biomass) are combusted for household heating in addition to daily energy consumption. Particularly in rural and suburban areas, solid fuels are burned in residential stoves without any emission controls and with a low combustion efficiency, making them likely to emit more primary carbonaceous particles[53,54]. It has been reported that residential solid fuel combustion accounted for 27% of the primary $PM_{2.5}$ in China[54]. In addition, fuel combustion is likely to be a large source of the high NH_3 in urban areas[55–57], which plays critical roles in buffering the aerosol pH and in acid–base reactions that generate secondary particles[58,59].

Under high humidity conditions, the combustion-emitted SO_2 and NOx can undergo atmospheric chemistry processes to transformed into SIAs. These enhanced SIAs contribute significantly to particle water uptake and trigger a robust positive feedback under elevated RH conditions (Fig. 5). The freshly emitted EC is hydrophobic and becomes hydrophilic after being aged in ambient air. The aging process of EC particles can bring water-soluble species to be surface coated and incorporated into aerosol droplets, and further promote the catalytic oxidation of SO_2 to sulfate under a high RH by reducing reaction barriers[24,60]. Aerosol water also enhances the aqueous formation of oxalate in Fe-containing particles[52], which age to particles containing Fe-oxalate complexes, serving as a contributor to N(III) generation. We propose that the oxidation of dissolved SO_2 by in-particle N(III), which likely generated through the heterogeneous reaction of NO_2 on surfaces of aged EC-containing, as well as the reaction between nitrate and Fe(II) promoted by photolysis of Fe-oxalate particles, dominated the rapid sulfate formation at an aerosol pH

of 4.0–4.5. This indicates that these two pathways are potential sources of the observed high HONO, which is a primary precursor of OH radicals[61], thereby potentially enhancing atmospheric oxidation capacity and accelerating secondary formation in winter. For SOA formation, we demonstrate that POAs originating from fossil fuel combustion potentially serve as precursors by acting as carriers for condensation and transformation of secondary organic species or reactants for aqueous-phase oxidation under high RH conditions. It should be noted that we could not specify the physical or chemical mechanisms behind this FC-POAs to SOAs transformation in this study. However, the results still imply that controlling POA emissions from fossil fuel combustion helps reduce the generation of SOAs under high RH levels.

In addition, the weakening effect of aged EC on haze mitigation is reflected not only in high humidity conditions but also in conditions of increasing O_3[62]. Considering these findings, we highlight that the effective mitigation of secondary aerosol formation in winter haze of northern China relies on reducing primary emissions, including multiple pollutants such as OAs, EC, transition metals, and reactive gases, from the combustion of fuels, particularly that of fossil fuels. These findings are also of great significance for winter haze pollution mitigation in areas with solid fuels combusted for heating, as well as in urban areas with high humidity.

METHODS

Sampling location and experimental methods

The field measurements were conducted from January 21 to February 10, 2022, in Tai'an City (36.21°N, 117.03°E), situated at the foot of Mount Tai in Shandong Province, China. The sampling site is surrounded by schools, residential and commercial districts, as well as traffic roads, making it a representative location for characterizing urban air pollution. Hourly measurements of water-soluble inorganic species (SO_4^{2-}, NO_3^-, NH_4^+, Cl^-, K^+, Na^+, Ca^{2+}, and Mg^{2+}) in $PM_{2.5}$ were performed using URG-9000D (Thermal Fisher Scientific, USA) equipped with two IC systems. Real-time data on particle size and chemical composition of single particles were obtained using SPAMS (Hexin Analytical Instrument Co., Ltd.,

China). The long-path differential optical absorption spectroscopy (LP-DOAS) technique was employed for the measurement of HONO. The target species in this study included atmospheric aerosols and gases ($PM_{2.5}$, SO_2, NO_2, CO, O_3, HONO, NH_3, and aerosol chemical components), and meteorological parameters were also measured (time series presented in Supplementary Fig. 1; instrument information provided in Supplementary Table 1). Further details regarding the URG-9000D, SPAMS and DOAS can be found in Sun et al.[63], Li et al.[64], and Nan et al.[65], respectively.

Particle type identification

The ambient particles were categorized into distinct particle categories based on the SPAMS spectral characteristics using an adaptive resonance theory method (ART-2) with a vigilance factor of 0.8 and a learning rate of 0.05 over 20 iterations implemented in MATLAB. We identified 10 categories comprising 27 subclasses of particles: ECOC, EC, Fe-rich, Cu-rich, K-CN, K-Ca, K-NH4, K-rich, NaK-carbon, and NaK particles. These particles had diverse sources and formation pathways and exhibited distinct mass spectral signatures, particle sizes, and temporal variations. The number fraction and average mass spectra of these particle types are comprehensively presented in Supplementary Table 2, and Supplementary Figs. 1 and 2. The suffixes -sec and -nit denote particles with prominent secondary inorganic species ($-97[HSO_4^-]$ and $-62[NO_3^-]$) and nitrate ($-62[NO_3^-]$ and $-46[NO_2^-]$), respectively, representing aged particles. Here, we describe the identification basis for several representative particles.

The HSO4 particles were defined as those containing $-97[HSO_4^-]$ and $-96[SO_4^-]$, and the NO3 particles were defined as those containing $-62[NO_3^-]$. HMS-containing particles were identified by the presence of a peak at $m/z = -111$, with relative peak areas exceeding 0.2% (Supplementary Fig. 4). We excluded the possibility of m/z -111 being attributed to methylsulfate ($CH_3OSO_3^-$), which is more likely to form under highly acid and extremely low-temperature conditions[42,66].

The ECOCCN particles exhibit a high intensity of carbonaceous fragments in the positive mass spectrum, and prominent $-26[CN^-]$, $-97[HSO_4^-]$, and EC fragments in the negative mass spectrum. These particles are identified as POAs directly emitted from the combustion of fossil fuels (referred to as FC-POAs), either in particulate form or condensed into the particle phase without undergoing chemical transformations[67]. This identification is based on their small particle size (Supplementary Fig. 3), negative correlations between their number fraction and RH ($r = -0.405$, $p < 0.05$ by two-tailed t-test), sulfate-rich composition, and strong association with PAHs fragments (i.e., m/z $-25[C_2H^-]$ and $-49[C_4H^-]$)[12,68] (Supplementary Fig. 8).

The KOCCN particles represent freshly emitted POAs from biomass burning, as indicated by the dominant peaks of $+39[K^+]$, organic fragments, $-26[CN^-]$, and $-42[CNO^-]$, along with certain levoglucosan fragments such as $-45[CHO_2^-]/-59[C_2H_3O_2^-]$ / $-73[C_3H_5O_2^-]$, and a lower intensity of $-62[NO_3^-]$ and $-46[NO_2^-]$ than $-97[HSO_4^-]$[69]. Moreover, the number of KOCCN particle was independent of the RH and correlated well with the number of fire points (Supplementary Fig. 9). Therefore, the total combustion-derived POAs consist of ECOCCN and KOCCN particles.

The ECOC-sec particles exhibit larger particle sizes and are characterized by a prominent abundance of carbonaceous fragments in the positive mass spectrum, as well as a higher peak of $-62[NO_3^-]$ than $-97[HSO_4^-]$ in the negative spectrum, suggesting that these combustion-derived particles have undergone atmospheric aging processes. The subclass of ECOC-sec particles, which is rich in HMS, is referred to as ECOC-HMS particles. The ECOC-sec particles can be identified as SOAs due to their tendency to mix with oxidized organic species and HMS, as

well as their positive response to increasing LWC. Further discussion on this identification is provided in the main text.

Classification of fuel combustion-derived particles

Here, 15 types of EC-containing particles were extracted, the mass spectra of which exhibit the signals of apparent EC fragments. This is an important basis for identifying the combustion origin of particles since EC is exclusively derived from incomplete fuel combustion. According to the particle sizes and mass spectrum signatures (Fig. 1d, and Supplementary Figs. 2 and 3), we further classified the EC-containing particles into four categories: EC-fresh (EC particles mixed with little organics and nitrate), EC-aged (containing abundant nitrate and sulfate), ECOC-fresh (with organics but minimal amounts of nitrate), and ECOC-aged particles (containing organics and abundant nitrate and sulfate). The EC-fresh and ECOC-fresh represent fresh EC-containing particles characterized by a significant $-26[CN^-]$ peak and smaller particle size (mainly 100–900 nm), while the EC-aged and ECOC-aged particles were aged EC-containing particles, distinguished by a larger particle size and more secondary species, particularly nitrate.

$$N_{EC-fresh} = N_{ECpure} + N_{KCaECCN} + N_{KECCN} + N_{NaKECCN} \quad (6)$$

$$N_{EC-aged} = N_{EC-sec} + N_{EC-nit} + N_{NaKEC} \quad (7)$$

$$N_{ECOC-fresh} = N_{ECOCCN} + N_{KOCCN} \quad (8)$$

$$N_{ECOC-aged} = N_{ECOC-sec} + N_{ECOC-nit} + N_{KNH4ECOC} + N_{NaKECOC} \quad (9)$$

Here, ECOC-sec and EC-sec include ECOC-HMS and EC-HMS, respectively, as well as in the main text.

Prediction of LWC and pH using ISORROPIA-II model

The aerosol LWC and pH values were predicted using the ISORROPIA-II aerosol thermodynamic equilibrium model[34], with one-hour resolution of aerosol inorganic species (SO_4^{2-}, NO_3^-, NH_4^+, Cl^-, K^+, Na^+, Ca^{2+}, and Mg^{2+}) and gaseous NH_3 as input data. We performed this model simulation in forward mode and based on the assumption of a metastable phase state. The aerosol pH was calculated as follows:

$$pH = -\log_{10}\left(\frac{1000H_{air}^+}{LWC}\right). \quad (10)$$

where H_{air}^+ and LWC are denoted in units of µg m^{-3}. Here, LWC represents the aerosol liquid water associated solely with the inorganic species, assuming a negligible contribution from organic components. In this study, the LWC derived from the organic fraction, estimated following the same approach used by Cheng et al.[3], was only 2.5% of that from the inorganic fraction.

Calculation of the fraction of SOAs generated from FC-POAs

The ECOC-sec particles (identified as SOAs) may have mainly originated from gas-particle partitioning and aqueous-phase oxidation of semi-volatile organic compounds on the EC particles, as well as aqueous processes of ECOCCN particles (namely FC-POAs). It is plausible to assume that ECOCCN particles served as the solely POA source of ECOC-sec particles, while other particles were not assumed. For instance, the positive spectrum of K- particles exhibited only a minimal amount of EC fragments, which could not be secondarily formed after aging. Therefore, K- particles cannot undergo transformation into ECOC-sec particles. In addition, further aging of the ECOC-sec particles, such as the loss of organic coating mass and transformation into EC-sec, was not considered because the process of losing coating mass is time-consuming[70].

The method for calculating the fraction of SOAs generated from POAs (denoted as $f_{FC-POA \ origin \ for \ SOA}$) was as follows. As depicted

in Supplementary Fig. 1, during Cp with a low RH of 32%, the average numbers of ECOCCN and ECOC-sec particles were merely 243 and 61, respectively. This indicates that aqueous processes leading to the formation of FC-POAs may not have taken place, and there was almost no FC-POA origin for SOAs. Assuming a similar scenario as Cp period, where no transformation from FC-POAs to SOAs took place in the other period, we can calculate the particle number for hypothetical FC-POAs (denoted as N^*_{FC-POA}, representing the total POAs directly emitted from fossil fuel combustion without transformation) using the following approach.

$$N*_{FC-POA} = (N_{ECOCCN} + N_{ECOC-sec}) \times \left(\frac{N_{ECOCCN}}{N_{ECOCCN} + N_{ECOC-sec}} \right)_{Cp} \tag{11}$$

Then, the $f_{FC-POA \text{ origin for SOA}}$ can be calculated as follows:

$$f_{FC-POA \text{ origin for SOA}} = \frac{N*_{FC-POA} - N_{ECOCCN}}{N_{ECOC-sec}} \tag{12}$$

Supplementary Fig. 10 demonstrates that the calculated N^*_{FC-POA} correlated well with the EC, CO, and OC mass concentrations, thus confirming the reliability of the assumptions and calculations.

DATA AVAILABILITY

All data needed to evaluate the conclusions in the paper are present in the paper and/or the Supplementary Information. Additional data related to this paper are available on request by contacting the corresponding author Jianmin Chen (jmchen@fudan.edu.cn).

REFERENCES

1. Geng, G. et al. Impact of China's Air Pollution Prevention and Control Action Plan on PM$_{2.5}$ chemical composition over eastern China. Science China Earth Sciences. *SCIENTIA SINICA Terra.* **62**, 469–482 (2020).
2. Zheng, Y. et al. Precursors and pathways leading to enhanced secondary organic aerosol formation during severe haze episodes. *Environ. Sci. Technol.* **55**, 15680–15693 (2021).
3. Cheng, Y. et al. Reactive nitrogen chemistry in aerosol water as a source of sulfate during haze events in China. *Sci. Adv.* **2**, e1601530 (2016).
4. Gkatzelis, G. I. et al. Uptake of water-soluble gas-phase oxidation products drives organic particulate pollution in Beijing. *Geophys. Res. Lett.* **48**, 1–12 (2021).
5. Shah, V. et al. Chemical feedbacks weaken the wintertime response of particulate sulfate and nitrate to emissions reductions over the eastern United States. *Proc. Natl Acad. Sci. USA* **115**, 8110–8115 (2018).
6. Li, H. et al. Mechanistic study of the aqueous reaction of organic peroxides with HSO$_3^-$ on the surface of a water droplet. *Angew. Chem.* **133**, 20362–20365 (2021).
7. Liu, T., Chan, A. W. H. & Abbatt, J. P. D. Multiphase oxidation of sulfur dioxide in aerosol particles: implications for sulfate formation in polluted environments. *Environ. Sci. Technol.* **55**, 4227–4242 (2021).
8. Wang, W. et al. Sulfate formation is dominated by manganese-catalyzed oxidation of SO$_2$ on aerosol surfaces during haze events. *Nat. Commun.* **12**, 1–10 (2021).
9. Harris, E. et al. Enhanced role of transition metal ion catalysis during in-cloud oxidation of SO$_2$. *Science* **340**, 727–730 (2013).
10. Nie, W. et al. Secondary organic aerosol formed by condensing anthropogenic vapours over China's megacities. *Nat. Geosci.* **15**, 255–261 (2022).
11. Mcneill, V. F. Aqueous organic chemistry in the atmosphere: sources and chemical processing of organic aerosols. *Environ. Sci. Technol.* **49**, 1237–1244 (2015).
12. Wang, J. et al. Aqueous production of secondary organic aerosol from fossil-fuel emissions in winter Beijing haze. *Proc. Natl Acad. Sci. USA* **118**, 1–6 (2021).
13. Zhang, R. Y. et al. Formation of urban fine particulate matter. *Chem. Rev.* **115**, 3803–3855 (2015).
14. Xu, B. et al. Large contribution of fossil-derived components to aqueous secondary organic aerosols in China. *Nat. Commun.* **13**, 1–12 (2022).
15. Shiraiwa, M. et al. Global distribution of particle phase state in atmospheric secondary organic aerosols. *Nat. Commun.* **8**, 1–7 (2017).
16. Ravishankara, A. R. Heterogeneous and multiphase chemistry in the troposphere. *Science* **276**, 1058–1065 (1997).
17. Xu, Y. et al. Aerosol liquid water promotes the formation of water-soluble organic nitrogen in submicrometer aerosols in a suburban forest. *Environ. Sci. Technol.* **54**, 1406–1414 (2020).
18. Wong, J. P. S., Lee, A. K. Y. & Abbatt, J. P. D. Impacts of sulfate seed acidity and water content on isoprene secondary organic aerosol formation. *Environ. Sci. Technol.* **49**, 13215–13221 (2015).
19. Faust, J. A., Wong, J. P. S., Lee, A. K. Y. & Abbatt, J. P. D. Role of aerosol liquid water in secondary organic aerosol formation from volatile organic compounds. *Environ. Sci. Technol.* **51**, 1405–1413 (2017).
20. Wu, Z. et al. Aerosol liquid water driven by anthropogenic inorganic salts: implying its key role in haze formation over the North China Plain. *Environ. Sci. Technol. Lett.* **5**, 160–166 (2018).
21. Wang, J. et al. Fast sulfate formation from oxidation of SO$_2$ by NO$_2$ and HONO observed in Beijing haze. *Nat. Commun.* **11**, 1–7 (2020).
22. Wang, T. et al. Sulfate formation apportionment during winter haze events in North China. *Environ. Sci. Technol.* **56**, 7771–7778 (2022).
23. Yang, J. et al. Unraveling a new chemical mechanism of missing sulfate formation in aerosol haze: gaseous NO$_2$ with aqueous HSO$_3^-$/SO$_3^{2-}$. *J. Am. Chem. Soc.* **141**, 19312–19320 (2019).
24. Zhang, F. et al. An unexpected catalyst dominates formation and radiative forcing of regional haze. *Proc. Natl Acad. Sci. USA* **117**, 3960–3966 (2020).
25. Li, J. et al. A more important role for the ozone-S(IV) oxidation pathway due to decreasing acidity in clouds. *J. Geophys. Res. Atmos.* **125**, 1–13 (2020).
26. Li, J. et al. The evolution of cloud and aerosol microphysics at the summit of Mt. Tai, China. *Atmos. Chem. Phys.* **20**, 13735–13751 (2020).
27. Liu, Y., Yan, C. & Zheng, M. Source apportionment of black carbon during winter in Beijing. *Sci. Total Environ.* **618**, 531–541 (2018).
28. Chen, B. et al. Source forensics of black carbon aerosols from China. *Environ. Sci. Technol.* **47**, 9102–9108 (2013).
29. Han, Y. et al. Evaluation of the thermal/optical reflectance method for discrimination between char- and soot-EC. *Chemosphere* **69**, 569–574 (2007).
30. Gen, M., Zhang, R. & Chan, C. K. Nitrite/nitrous acid generation from the reaction of nitrate and Fe(II) promoted by photolysis of iron−organic complexes. *Environ. Sci. Technol.* **55**, 15715–15723 (2021).
31. Liu, Y. et al. Submicrometer particles are in the liquid state during heavy haze episodes in the urban atmosphere of Beijing, China. *Environ. Sci. Technol. Lett.* **4**, 427–432 (2017).
32. Shiraiwa, M., Ammann, M., Koop, T. & Pöschl, U. Gas uptake and chemical aging of semisolid organic aerosol particles. *Proc. Natl Acad. Sci. USA* **108**, 11003–11008 (2011).
33. Seinfeld, J. H. & Pandis, S. N. *Atmospheric Chemistry and Physics: From Air Pollution to Climate Change* 274–310 (John Wiley & Sons, Inc., 2016).
34. Fountoukis, C. & Nenes, A. ISORROPIA II: a computationally efficient thermodynamic equilibrium model for K$^+$-Ca^{2+}-Mg^{2+}-NH$_4^+$-Na$^+$-SO$_4^{2-}$-NO$_3^-$-Cl$^-$-H$_2$O aerosols. *Atmos. Chem. Phys.* **7**, 4639–4659 (2007).
35. Song, M. et al. Comparison of phase states of PM$_{2.5}$ over megacities, Seoul and Beijing, and their implications on particle size distribution. *Environ. Sci. Technol.* **56**, 17581–17590 (2022).
36. Liu, Y. et al. Aerosol phase state and its link to chemical composition and liquid water content in a subtropical coastal megacity. *Environ. Sci. Technol.* **53**, 5027–5033 (2019).
37. Fang, Y. et al. Relative humidity and O$_3$ concentration as two prerequisites for sulfate formation. *Atmos. Chem. Phys.* **19**, 12295–12307 (2019).
38. Huang, R. J. et al. Contrasting sources and processes of particulate species in haze days with low and high relative humidity in wintertime Beijing. *Atmos. Chem. Phys.* **20**, 9101–9114 (2020).
39. Pay, M. T., Jiménez-Guerrero, P. & Baldasano, J. M. Assessing sensitivity regimes of secondary inorganic aerosol formation in Europe with the CALIOPE-EU modeling system. *Atmos. Environ.* **51**, 146–164 (2012).
40. Whiteaker, J. R. & Prather, K. A. Hydroxymethanesulfonate as a tracer for fog processing of individual aerosol particles. *Atmos. Environ.* **37**, 1033–1043 (2003).
41. Gilardoni, S. et al. Direct observation of aqueous secondary organic aerosol from biomass-burning emissions. *Proc. Natl Acad. Sci. USA* **113**, 10013–10018 (2016).
42. Lee, S. H., Murphy, D. M., Thomson, D. S. & Middlebrook, A. M. Nitrate and oxidized organic ions in single particle mass spectra during the 1999 Atlanta Supersite Project. *J. Geophys. Res. Atmos.* **108**, 1–8 (2003).
43. Campbell, J. R. et al. Source and chemistry of hydroxymethanesulfonate (HMS) in Fairbanks, Alaska. *Environ. Sci. Technol.* **56**, 7657–7667 (2022).
44. Chen, C. et al. The importance of hydroxymethanesulfonate (HMS) in winter haze episodes in North China Plain. *Environ. Res.* **211**, 113093 (2022).

45. Song, S. et al. Possible heterogeneous chemistry of hydroxymethanesulfonate (HMS) in northern China winter haze. *Atmos. Chem. Phys.* **19**, 1357–1371 (2019).
46. Ma, T. et al. Contribution of hydroxymethanesulfonate (HMS) to severe winter haze in the North China Plain. *Atmos. Chem. Phys.* **5**, 5887–5897 (2020).
47. Dovrou, E. et al. Measurement techniques for identifying and quantifying hydroxymethanesulfonate (HMS) in an aqueous matrix and particulate matter using aerosol mass spectrometry and ion chromatography. *Atmos. Meas. Tech.* **12**, 5303–5315 (2019).
48. Wei, L. et al. Quantitative determination of hydroxymethanesulfonate (HMS) using ion chromatography and UHPLC-LTQ-orbitrap mass spectrometry: a missing source of sulfur during haze episodes in Beijing. *Environ. Sci. Technol. Lett.* **7**, 701–707 (2020).
49. Yu, J. Z. An interfacial role for NO_2. *Nat. Chem.* **13**, 1157–1163 (2021).
50. Wang, G. et al. Persistent sulfate formation from London Fog to Chinese haze. *Proc. Natl Acad. Sci. USA* **113**, 13630–13635 (2016).
51. Khalizov, A. F., Cruz-Quinones, M. & Zhang, R. Heterogeneous reaction of NO_2 on fresh and coated soot surfaces. *J. Phys. Chem. A* **114**, 7516–7524 (2010).
52. Zhang, G. et al. Oxalate formation enhanced by Fe-containing particles and environmental implications. *Environ. Sci. Technol.* **53**, 1269–1277 (2019).
53. Zhang, J. et al. Exploring wintertime regional haze in northeast China: role of coal and biomass burning. *Atmos. Chem. Phys.* **20**, 5355–5372 (2020).
54. Yun, X. et al. Residential solid fuel emissions contribute significantly to air pollution and associated health impacts in China. *Sci. Adv.* **6**, 1–8 (2020).
55. Chen, Z. et al. Significant contributions of combustion-related sources to ammonia emissions. *Nat. Commun.* **13**, 7710 (2022).
56. Pan, Y. et al. Source apportionment of aerosol ammonium in an ammonia-rich atmosphere: an isotopic study of summer clean and hazy days in urban Beijing. *J. Geophys. Res. Atmos.* **123**, 5681–5689 (2018).
57. Wang, Y. et al. Vehicular ammonia emissions significantly contribute to urban $PM_{2.5}$ pollution in two Chinese megacities. *Environ. Sci. Technol.* **57**, 2698–2705 (2023).
58. Zheng, G. et al. Multiphase buffer theory explains contrasts in atmospheric aerosol acidity. *Science* **369**, 1374–1377 (2020).
59. Huang, X., Zhang, J., Zhang, W., Tang, G. & Wang, Y. Atmospheric ammonia and its effect on $PM_{2.5}$ pollution in urban Chengdu, Sichuan Basin, China. *Environ. Pollut.* **291**, 118195 (2021).
60. He, G., Ma, J. & He, H. Role of carbonaceous aerosols in catalyzing sulfate formation. *ACS Catal.* **8**, 3825–3832 (2018).
61. Xue, C. et al. HONO budget and its role in nitrate formation in the rural North China Plain. *Environ. Sci. Technol.* **54**, 11048–11057 (2020).
62. Zhang, Y., Zhang, Q., Wu, N. & Ding, A. Weakened haze mitigation induced by enhanced aging of black carbon in China. *Environ. Sci. Technol.* **56**, 7629–7636 (2022).
63. Sun, J. et al. Secondary inorganic ions characteristics in $PM_{2.5}$ along offshore and coastal areas of the megacity Shanghai. *J. Geophys. Res. Atmos.* **126**, 1–16 (2021).
64. Li, L. et al. Real time bipolar time-of-flight mass spectrometer for analyzing single aerosol particles. *Int J. Mass Spectrom.* **303**, 118–124 (2011).
65. Nan, J., Wang, S., Guo, Y., Xiang, Y. & Zhou, B. Study on the daytime OH radical and implication for its relationship with fine particles over megacity of Shanghai, China. *Atmos. Environ.* **154**, 167–178 (2017).
66. Kane, S. M. & Leu, M. T. Uptake of methanol vapor in sulfuric acid solutions. *J. Phys. Chem. A* **105**, 1411–1415 (2001).
67. Sharma, N. et al. *Air Pollution and Control: Energy, Environment, and Sustainability* 109–116 (Springer Nature Singapore Pte Ltd., 2018).
68. Spencer, M. T., Shields, L. G., Sodeman, D. A., Toner, S. M. & Prather, K. A. Comparison of oil and fuel particle chemical signatures with particle emissions from heavy and light duty vehicles. *Atmos. Environ.* **40**, 5224–5235 (2006).
69. Bi, X. et al. Mixing state of biomass burning particles by single particle aerosol mass spectrometer in the urban area of PRD, China. *Atmos. Environ.* **45**, 3447–3453 (2011).
70. Sedlacek, A. J. et al. Using the black carbon particle mixing state to characterize the lifecycle of biomass burning aerosols. *Environ. Sci. Technol.* **56**, 14315–14325 (2022).

AUTHOR CONTRIBUTIONS

J.C. and Y.G. conceived the initial idea and designed the study. X.H. and Z.L. performed the field experiments and with inputs from all coauthors. X.H. conducted the data analysis and drafted/revised the manuscript. B.Z., S.Y., L.X., X.W., H.F., L.W., C.G., and A.M. provided the supervision for the analysis and interpretation of data. J.C., Q.L., and X.W. contributed the editing and revision the manuscript.

COMPETING INTERESTS

The authors declare no competing interests.

ADDITIONAL INFORMATION

Supplementary information The online version contains supplementary material available at https://doi.org/10.1038/s41612-023-00504-1.

Correspondence and requests for materials should be addressed to Yanzhen Ge or Jianmin Chen.

Reprints and permission information is available at http://www.nature.com/reprints

Publisher's note Springer Nature remains neutral with regard to jurisdictional claims in published maps and institutional affiliations.